cosmetics

MDPI

Article

Anti-Glycation and Well-Ageing Effects of *Inula britannica* Flower Extract: From AGEs-RAGE Signalling to a Vehicle-Controlled Split-Face Study

Yina Lu [1,2], Fei Zhou [2], Xinqiang Li [2], Liujie Xu [2], Zheng Yan [3] and Feng-Qing Wang [1,*]

[1] School of Biotechnology, East China University of Science and Technology, Shanghai 200237, China; inna_lu@jakabiotech.com
[2] Technology Innovation Center, JAKA Biotech. Co., Ltd., Shanghai 201507, China
[3] School of Bioengineering, Beijing Polytechnic University, Beijing 100176, China
* Correspondence: fqwang@ecust.edu.cn

Abstract

Objective: This study was conducted to characterize an *Inula britannica* L. flower extract (IB) and evaluate its anti-glycation and anti-ageing effects on Methylglyoxal (MGO)-challenged human dermal fibroblasts via a vehicle-controlled split-face study. **Methods:** The extract was prepared after characterization via high-performance liquid chromatography (HPLC) and ultraviolet (UV) detection. MGO-challenged UVAP7 fibroblasts were assessed for Nε-(carboxymethyl) lysine (CML), the receptor for advanced glycation end-products (RAGE), nuclear factor kappa-B (NF-κB), interleukin (IL)-6, IL-8, and senescence-associated markers of β-galactosidase, p16, and Lamin B1 via flow cytometry, Western blotting, enzyme-linked immunosorbent assay, and quantitative real-time PCR. Cross-sectional datasets of facial skin autofluorescence (n = 114) and Commission Internationale de l'Éclairage (CIE) b* (n = 162) were used to model their associations with chronological age. A 56-day, participant-blinded split-face study involving 36 adults was performed to evaluate the anti-glycation and well-ageing effect of a topical formulation containing 0.5% IB or its vehicle. **Results:** The total phenol content in IB reached 3.0–4.0% using the UV method, consisting of many caffeoyls from the HPLC analysis. At 0.016%, IB significantly inhibited MGO-induced positive cells of CML and RAGE by 82.97% and 96.69%, respectively; the total abundance of NF-κB protein was reduced by 90.32%; and cytokine secretion and senescence-associated markers improved. Age was positively associated with skin autofluorescence of AGEs (R^2 = 0.8003) and CIE b* values (R^2 = 0.5464). In the split-face study, at day 56, when compared to the vehicle-treated side, the IB-treated side showed significantly lower skin autofluorescence of AGEs, CIE b* values, under-eye wrinkle scores, and crow's feet scores, but a higher high-intensity dermal echo parameter. Using the age-equivalent estimates derived from a population regression model, the effects of post-IB treatment on skin AGEs and yellowness showed a reduction when compared to pre-IB treatment. **Conclusions:** IB attenuates MGO-induced glycation and senescence-related responses in dermal fibroblasts through the AGE-RAGE pathway to improve skin yellowness, echogenicity, and periocular wrinkles. These findings support further investigation of chemically standardized IB and its potential application in skin ageing.

Keywords: *Inula britannica* flower extract; advanced glycation end-products; glycation; skin ageing; skin yellowness

Check for updates

Academic Editor: Lucia Montenegro

Received: 14 October 2026
Revised: 3 November 2026
Accepted: 16 November 2026
Published: 19 November 2026

Copyright: © 2026 by the authors. Licensee MDPI, Basel, Switzerland. This article is an open access article distributed under the terms and conditions of the Creative Commons Attribution (CC BY) license.

1. Introduction

Skin ageing reflects intrinsic ageing and cumulative environmental exposure [1,2]. Non-enzymatic glycation contributes through reactions of reducing sugars or reactive carbonyl species with long-lived dermal proteins, forming advanced glycation end-products (AGEs) [3,4]. Glycation and cross-linking of collagen and elastin stiffen the extracellular matrix and are associated with reduced elasticity, yellowing, and wrinkling; Nε-(carboxymethyl) lysine (CML) is widely used as a marker of glycoxidative damage [5–9]. AGE and the receptor for AGEs (RAGE) signalling can activate nuclear factor kappa-B (NF-κB) and increase pro-inflammatory mediators, including interleukin (IL)-6 and IL-8 [10–15]. Increased senescence-associated β-galactosidase (SA-β-gal) activity and p16 expression and loss of Lamin B1 (LMNB1) are established as senescence-associated features [16,17]. These processes provide complementary targets for interventions against glycation-associated skin ageing [18].

Plant-derived phenolics may inhibit glycation through antioxidant, metal-chelating, and reactive-dicarbonyl-trapping activities [19–22]. *Inula britannica* L. has a history of medicinal use, and phytochemical studies of its flowers and aerial parts have identified terpenoids, flavonoids, and caffeic acid-derived phenolics [23–26]. Two earlier studies suggest its skin-related activity. Flower extracts modulated melanogenesis, hyaluronan-synthesis genes, and inflammatory genes in cultured cells [27], whereas total flower flavonoids improved antioxidant and structural skin measures in a D-galactose-induced mouse model [28]. Neither study examined Methylglyoxal (MGO)-induced glycation RAGE signalling in human dermal fibroblasts nor tested a topical formulation against a matched vehicle for skin yellowness and ageing. *Inula britannica* flower extract (IB), derived from the traditional medicinal plant using affinity chromatography, has emerged as a promising candidate targeting AGEs accumulation. In this study, a novel model of MGO-challenged UVAP7 fibroblasts was established to examine the relationship between ageing and glycation. Then, cross-sectional datasets were used to model the associations of facial skin autofluorescence AGEs and Commission Internationale de l'Éclairage (CIE) b* values with age. A 56-day, participant-blinded, vehicle-controlled split-face study was ultimately used to investigate the correlation between cellular regulatory effects and physiological improvements in skin, thereby substantiating the efficacy of formulas containing 0.5% IB. These mechanistic analyses establish a scientific foundation for IB's potential application in anti-glycation and well-ageing formulations. It also provides a hypothesis and data for IB's total phenols and effects on AGEs–RAGE pathways.

2. Materials and Methods

2.1. Preparation and Identification of IB

Fresh *Inula britannica* flowers were immersed in an aqueous ethanol solution for crude extraction. The resulting extract was concentrated, followed by affinity chromatography. Briefly, after adjusting the pH of the extract to 3.0–4.0, it was injected into a chromatography column containing anion exchange resin, and then into the macroporous adsorption resin (Hanyu Resin, Xi'an, China) at a pH of 6.0–7.0. It was first washed with water and 15% ethanol and then eluted with 50–70% ethanol. After decolorization with activated carbon, the eluate was concentrated and dried to a low alcohol content. The IB powder was obtained using the eluate reconstituted in deionized water with the addition of hydroxypropyl cyclodextrin (Tongwang Biotech., Zibo, China) at a 1:9 mass ratio after spray drying. The chemical profile of the IB was investigated via ultra-high-performance liquid chromatography (UPLC)–high-resolution mass spectrometry (HRMS) (Suitai Parma., Shanghai, China), high-performance liquid chromatography (HPLC; Agilent, Santa Clara, CA, USA), and total phenol content determination using the Folin–Phenol method under UV detection.

The HPLC detection was carried out at a column temperature of 30 °C, with a wavelength of 327 nm and a flow rate of 1.0 mL/min, using a mobile phase of 0.1% formic acid and acetonitrile solution on an Agilent SB-C18 chromatographic column (4.6 mm × 250 mm, 5 µm). The content of 1,3-dicaffeoylquinic acid (CAS No. 30964-13-7; National Institutes for Food and Drug Control, Beijing, China), 1,5-dicaffeoylquinic acid (CAS No. 19870-46-3), isochlorogenic acid A (CAS No. 2450-53-5), isochlorogenic acid C (CAS No. 32451-88-0), and 2, 3, 4, 5-tetracaffeoyl glucaric acid (CAS No. 1419478-52-6) (Yuanye Bio-Technology, Shanghai, China) was calculated from the corresponding standard and standard curve.

2.2. Establishment of the Glycation Model on Fibroblasts

Primary fibroblasts were derived from discarded human foreskin tissue obtained following surgical circumcision, with ethical approval granted by the institutional review board (No. JIEC-2023-S70, approved by Ethics Committee of Jinshan Hospital, Fudan University at 30 October 2023). Cell isolation was performed according to established protocols [29]. The pellet was resuspended in high-glucose DMEM medium (BasalMedia Technologies, Shanghai, China) supplemented with 10% newborn calf serum (Gibco, Grand Island, NY, USA) and 1% Penicillin–Streptomycin–Amphotericin B (Beyotime, Shanghai, China), and 6×10^5 cells were seeded per culture dish to obtain the foreskin fibroblast (FF). P0 generation of FF was seeded in a 10 cm dish and irradiated every two days with UVA 14.4 J/cm^2 for 10 min under a UVASPOT system (Honle, Ammersee, Germany) in phosphate-buffered saline (PBS; Beyotime, Shanghai, China). The cells were cultured for 7 days and labelled as P1 after digesting and passaging. This operation was repeated until P6 cells (UVAP7) were obtained. UVAP7 cells were seeded into 96-well or 6-well plates and allowed to adhere overnight. Subsequently, cells were treated for 7 days with 0.8 mM methylglyoxal (MGO; Adamas-beta, Shanghai, China) alone or in combination with IB at final concentrations ranging from 0.001% to 0.032% (v/v, without cell toxicity), or with aminoguanidine (AG; Adamas-beta, Shanghai, China) at 0.032% (v/v, without cell toxicity) as a positive control. Culture medium was refreshed after 72 h. At the end of the treatment period, cells were washed with PBS and harvested for downstream analysis.

2.3. Flow Cytometric Measurement of CML and RAGE

Cell viability was assessed using the cell counting kit-8 (CCK-8; APExBIO, Houston, TX, USA) in 96-well plates. Briefly, 10 µL of CCK-8 reagent was added to each well containing 100 µL of culture medium, and cells were incubated at 37 °C for 2 h. The absorbance was measured at 450 nm using a microplate reader (Tecan, Männedorf, Switzerland). Cell viability was expressed as a percentage relative to the negative control group. Under the non-toxic dosage, cells in 6-well plates were collected and fixed with 4% paraformaldehyde, followed by permeabilization with 0.1% Triton X-100 and blocking with 10% goat serum. After incubation overnight at 4 °C with anti-CML or anti-RAGE antibodies (1:200 dilution; Abcam, Cambridge, UK), fluorescent secondary antibodies (1:500 dilution; Thermo Fisher, Waltham, MA, USA) were added for another 45 min of incubation. Samples were acquired on a FACS Celesta cytometer (BD Biosciences, San Jose, CA, USA) using 530 nm and 575 nm detection channels for Alexa Fluor 488 and phycoerythrin, respectively. Quadrant gating distinguished positive and negative populations. Positive cells were expressed as a percentage of the gated population, and fold changes were calculated relative to the untreated control. The inhibition rate was calculated as $[1 - (\text{Value}_{\text{sample}} - \text{Value}_{\text{Control}})/(\text{Value}_{\text{MGO}} - \text{Value}_{\text{Control}})]$.

2.4. Western Blotting Detection of NF-κB

Cells were lysed in RIPA buffer containing phenyl methyl sulfonyl fluoride (Beyotime, Shanghai, China), and protein was quantified using the bicinchoninic acid assay. After separation via SDS-PAGE (Tanon, Shanghai, China), proteins were transferred to polyvinylidene fluoride membranes using Power Blotter XL (Thermo Fisher, Waltham, MA, USA) under a 350 mA current for 1 h. After blocking, the cut membrane was incubated with anti-NF-κB antibodies (1:1000 dilution; Proteintech, Wuhan, China) or GAPDH antibodies (1:1000 dilution; Thermo Fisher, Waltham, MA, USA), followed by HRP-conjugated secondary antibodies (1:2000 dilution; Thermo Fisher, Waltham, MA, USA). GAPDH served as the loading control. Bands were detected via chemiluminescence, quantified using the ImageJ 1.52a software (National Institutes of Health, Bethesda, MD, USA), and normalized to GAPDH. The inhibition rate was calculated as described above.

2.5. ELISA Detection for IL-6 and IL-8

Culture supernatants were collected to detect the IL-6 and IL-8 contents according to the manufacturer's instructions for commercial ELISA kits (NeoBioscience, Shenzhen, China). The inhibition rate was calculated as previously mentioned.

2.6. Assessment of Cellular Senescence

Senescence-associated changes were assessed via SA-β-gal staining and quantitative real-time PCR. For SA-β-gal staining, cells were fixed with 4% paraformaldehyde for 20 min, washed twice with PBS, and incubated overnight at 37 °C with 200 µL of staining solution (Beyotime, Shanghai, China) per well. Images were acquired using an inverted microscope (Leica, Wetzlar, Germany), and the percentage of SA-β-gal-positive cells was calculated by counting positive and total cells in three representative fields (400x). Total RNA was extracted using a commercial kit and reverse-transcribed into cDNA using the PrimeScript RT reagent kit (TaKaRa, Otsu, Japan). After using SYBR Green chemistry (TaKaRa, Otsu, Japan) with a 20 µL reaction volume, the relative fold change in p16 and Lamin B1 was calculated using the $2^{-}\Delta\Delta Ct$ method relative to the untreated control, with GAPDH as the reference. The increase rate was calculated as $[\text{Value}_{\text{sample}}/\text{Value}_{\text{MGO}} - 1]$. The primer sequences were as follows: GAPDH, 5′-TGACAACTTTGGTATCGTGGAAGG-3′ and 5′-AGGCAGGGATGATGTTCTGGAGAG-3′; p16, 5′-ACCAGAGGCAGTAACCATGC-3′ and 5′-CCTGTAGGACCTTCGGTGAC-3′; LMNB1, 5′-AATGGGAGGCTGGGAGATGAT-3′ and 5′-TGGTTCTTCCAGATGAGGTCAGTT-3′.

2.7. Clinical Study Design

2.7.1. Study for Population Skin Yellowness and Ageing

An exploratory cross-sectional analysis used anonymized facial measurements collected in Shanghai, China, under ethics approval, JKC-2307-00039, granted by the Cosmetics Evaluation Ethics Committee of JAKA at 21 July 2023. Participants aged 20–70 years were grouped by decade. The datasets comprised 114 records of skin autofluorescence AGEs obtained with an AGE Reader (DiagnOptics, Groningen, The Netherlands) and 162 records of CIE b* values obtained with a SkinColorCatch device (Delfin, Finland). Ordinary least-squares regression was used to model each endpoint against age and to derive regression equations and coefficients of determination (R^2) for the descriptive interpretation of the intervention data.

2.7.2. Preparation of the Test Formulations

The active and vehicle products were matched oil-in-water emulsions containing water, humectants, emulsifiers, emollients, rheology modifiers, and preservatives. The active

formulation contained 0.5% (*w*/*w*) IB, while the vehicle contained 0.45% hydroxypropyl-β-cyclodextrin to match the carrier present in the extract. Both the oil and aqueous phases were independently heated to 80–85 °C, combined under controlled conditions, and homogenized. The rheology modifier was added during the cooling phase; subsequently, the active or vehicle component—along with other thermolabile ingredients—was incorporated at approximately 45 °C and mixed until a homogeneous dispersion was achieved.

2.7.3. Vehicle-Controlled Split-Face Study

A 56-day, participant-blinded, vehicle-controlled split-face study was conducted in Shanghai, China, according to the TREND 22-item checklist. The study protocol received ethical approval from the designated Cosmetics Testing Ethics Committee (Approval No. JKC-2412-00055 at 25 December 2024), and written informed consent was obtained from all participants prior to enrollment. Thirty-six healthy adult volunteers (19 females and 17 males; aged 22–60 years; mean age 40.56 ± 11.38 years) with clinically assessed facial yellowness and baseline wrinkle severity scores ≥3 (on a 9-point visual scale) at both the crow's feet and infraorbital regions were enrolled [30,31]. Following a pre-study occlusive patch test to confirm cutaneous tolerance, participants applied the test formulation to the left hemiface and the vehicle control to the right hemiface twice daily for 56 consecutive days, with clinical assessors non-blinded. Evaluations were performed at baseline (0 d) and after 14, 28, and 56 days of treatment. The endpoints included skin autofluorescence AGEs, the CIE b* value, and the high-intensity dermal echo parameter measured using DermaLab Combo (Cortex, Denmark); these tests were conducted in different designated areas with three repetitions, and visual scores for yellowness, wrinkles under-eye, and crow's feet were obtained by a blinded dermatologist. The change rate was calculated as [Value $_{14\text{ d or }28\text{ d or }56\text{ d}}$/Value $_{0\text{ d}}$ − 1]. Photos were taken using Vplus (Fuhuan Technology, Shanghai, China).

2.8. Statistical Analysis

All in vitro experiments were performed with a minimum of three biological replicates. The flow diagram of this study followed the PRISMA guidelines, and is shown in Figure 1. Data are presented as mean ± standard deviation (SD). Clinical data are reported as mean ± SEM in figures, and the normality of paired differences was assessed before hypothesis testing. For the cross-sectional analysis, ordinary least-squares regression followed by analysis of variance ANOVA was used to estimate the slope, 95% confidence interval, R^2 and p value. Age-equivalent estimates were post hoc and descriptive. A paired t-test was employed to conduct significance analysis between the vehicle group and the sample group, with α set at 0.05 and the data following a normal distribution. $p < 0.05$ (*, $^{\#}$) was considered statistically significant; $p < 0.01$ (**, $^{\#\#}$) and $p < 0.001$ (***, $^{\#\#\#}$) were considered highly significant.

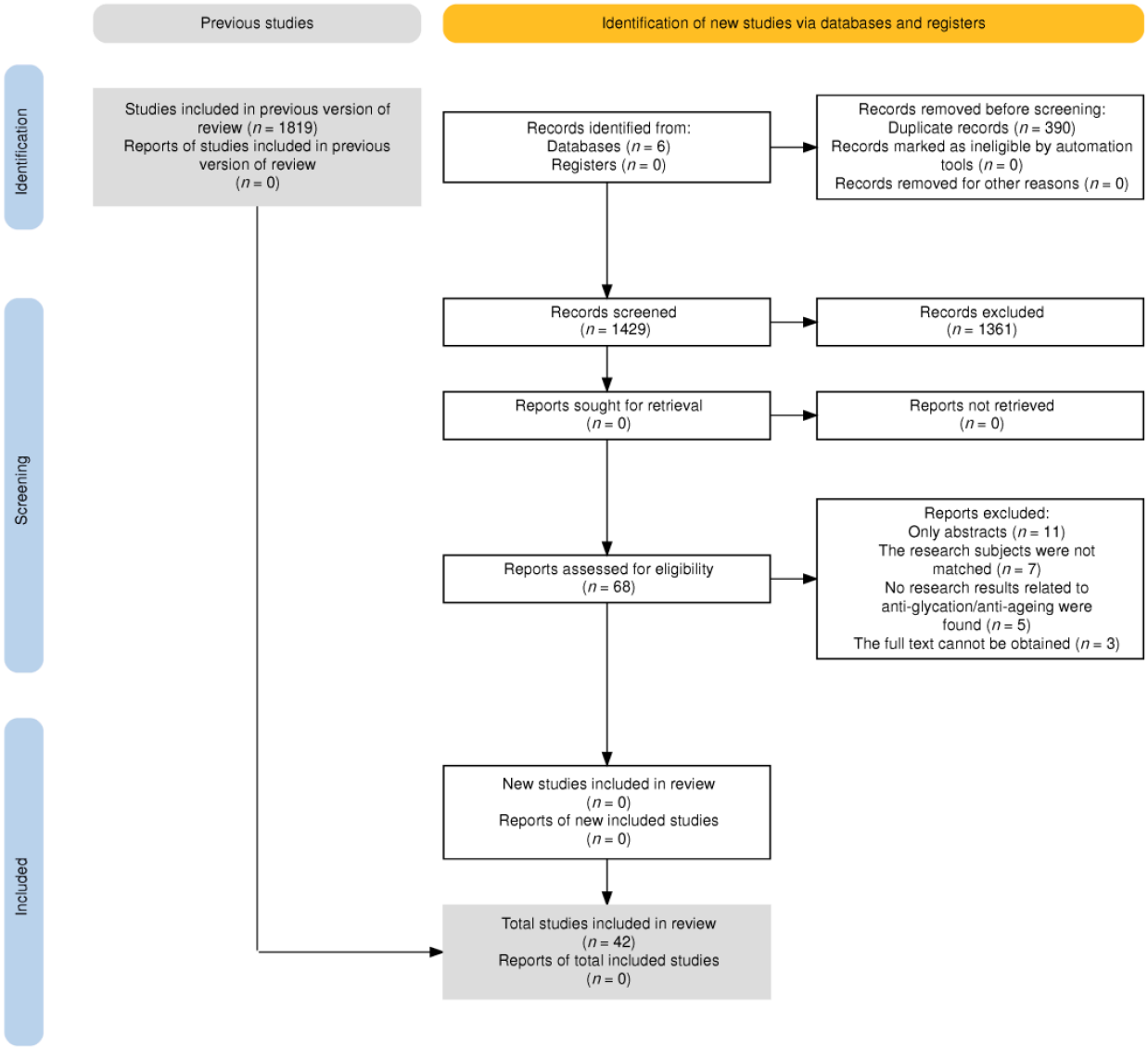
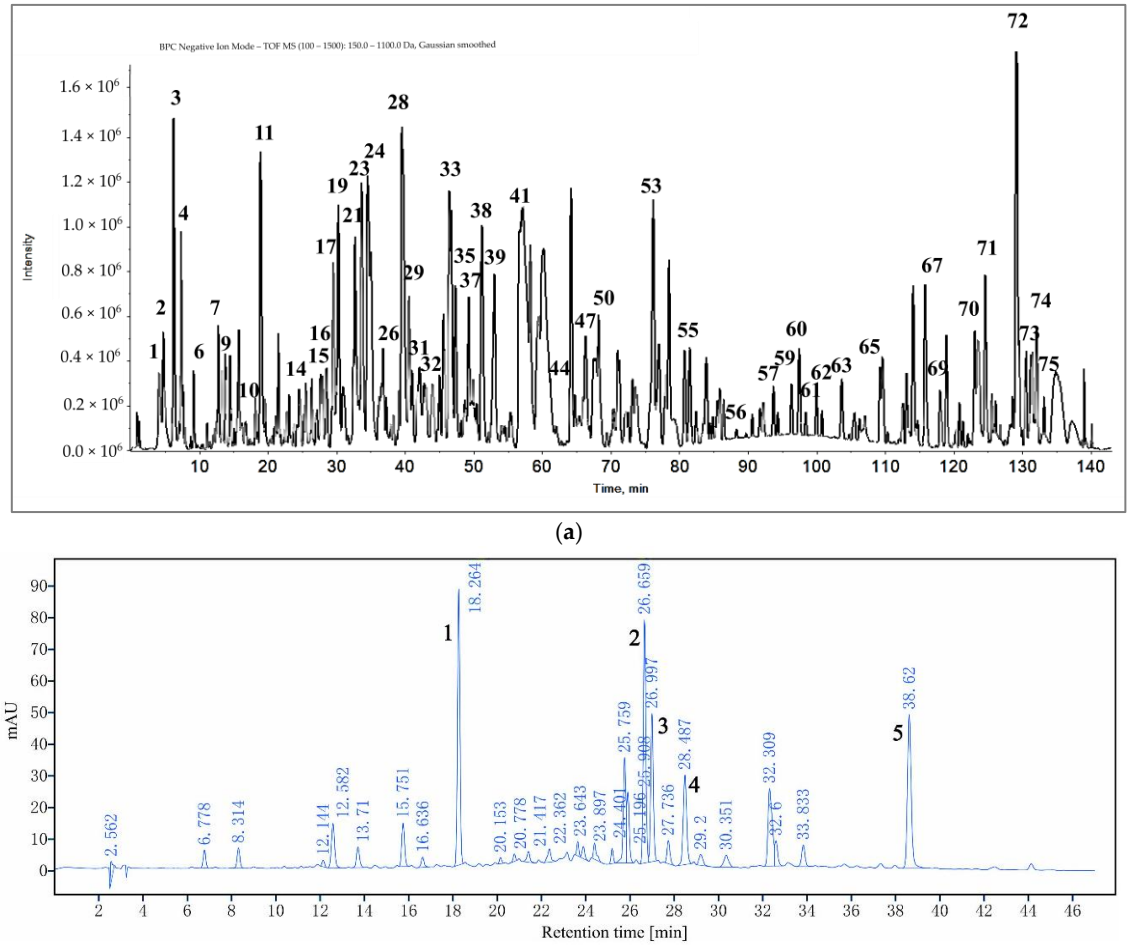


Figure 1. The flow diagram according to the PRISMA guidelines.

3. Results

3.1. Chemical Characterization of IB

At first, IB was subjected to UPLC-HRMS analysis for phytochemical profiling (Figure 2a), among which 75 phytochemicals and 22 phenols were identified. Relatively high absorption peaks at 3, 11, 19, 23, 24, and 28 belonged to phenolic compounds. Among them, 28 was identified as 1,3-dicaffeoylquinic acid. The total phenol content in IB reached 3.0–4.0% when using chlorogenic acid as the standard, mostly consisting of 1,3-dicaffeoylquinic acid (tR = 18.264 min), 1,5-dicaffeoylquinic acid (tR = 26.659 min), isochlorogenic acid A (tR = 26.997 min), isochlorogenic acid C (tR = 28.487 min), and 2, 3, 4, 5-tetracaffeoyl glucaric acid (tR = 38.62 min), as determined by the HPLC analysis and shown in Figure 2b. After multiple patches of IB analysis, the total phenol content was relatively stable, but the content of any single substance did not exceed 0.5% (*v*/*v*). The total content of the four isomers described above was 0.5 to 1.0% (with a R^2 value of the standard curve greater than 0.95, and a detection limit greater than 10 ppm).



(**a**)

(**b**)

Figure 2. Representative chromatogram of IB. (**a**) UPLC-HRMS Baseline Ion Current Plot (BPC)—Negative Ion Mode; 1 to 75 represent different phytochemicals; 28 is 1,3-Dicaffeoylquinic acid. (**b**) HPLC chromatogram at 327 nm. Peaks 1, 2, 3, 4, and 5 represent 1,3-dicaffeoylquinic acid, 1,5-dicaffeoylquinic acid, isochlorogenic acid A, isochlorogenic acid C, and 2, 3, 4, 5-tetracaffeoyl glucaric acid, respectively, with a total content of 0.6% to 1.2%.

3.2. Anti-Glycation Effects of IB Mediated by Inhibiting RAGE and NF-κB Expression

Glycation usually occurs in older individuals and is related to UV exposure. The extracellular matrix of the dermis layer of the skin is rich in collagen, elastin, and other proteins, making it susceptible to the accumulation of AGEs [8]. UVAP7 fibroblasts already exhibit photoageing and internal ageing-related characteristics [32], making them suitable for studies on cell glycation and senescence. MGO is an inducer of the glycation reaction, and it can increase AGE production in vitro [33]. As shown in Figure 3, after exposure to 0.8 mM MGO for 7 days, the proportions of CML- and RAGE-positive fibroblasts, as well as the total abundance of the NF-κB protein, were significantly increased when compared with the untreated control (NC) in UVAP7 cells. The downstream cytokines, including IL-6 and IL-8, also showed a significant increase in the culture medium. For IB and AG, it was non-toxic at 0.032% compared to MGO treatment (cell viability was 82.90% with $p = 0.068$) but showed significant inhibition of both AGEs content and signalling factors, while the vehicle control of hydroxypropyl cyclodextrin had no significant effect. At 0.016%, the inhibition rate was 82.97% for CML and 96.69% for RAGE, and it reached 90.32%, 77.85%, and 82.90% for NF-κB, IL-6, and IL-8, respectively. At 0.008%, the inhibition rate was similar to that at 0.016%, which may have been caused by the complex extract and the maximum inhibitory effect at high concentrations, as well as the duplicates in the experiment.

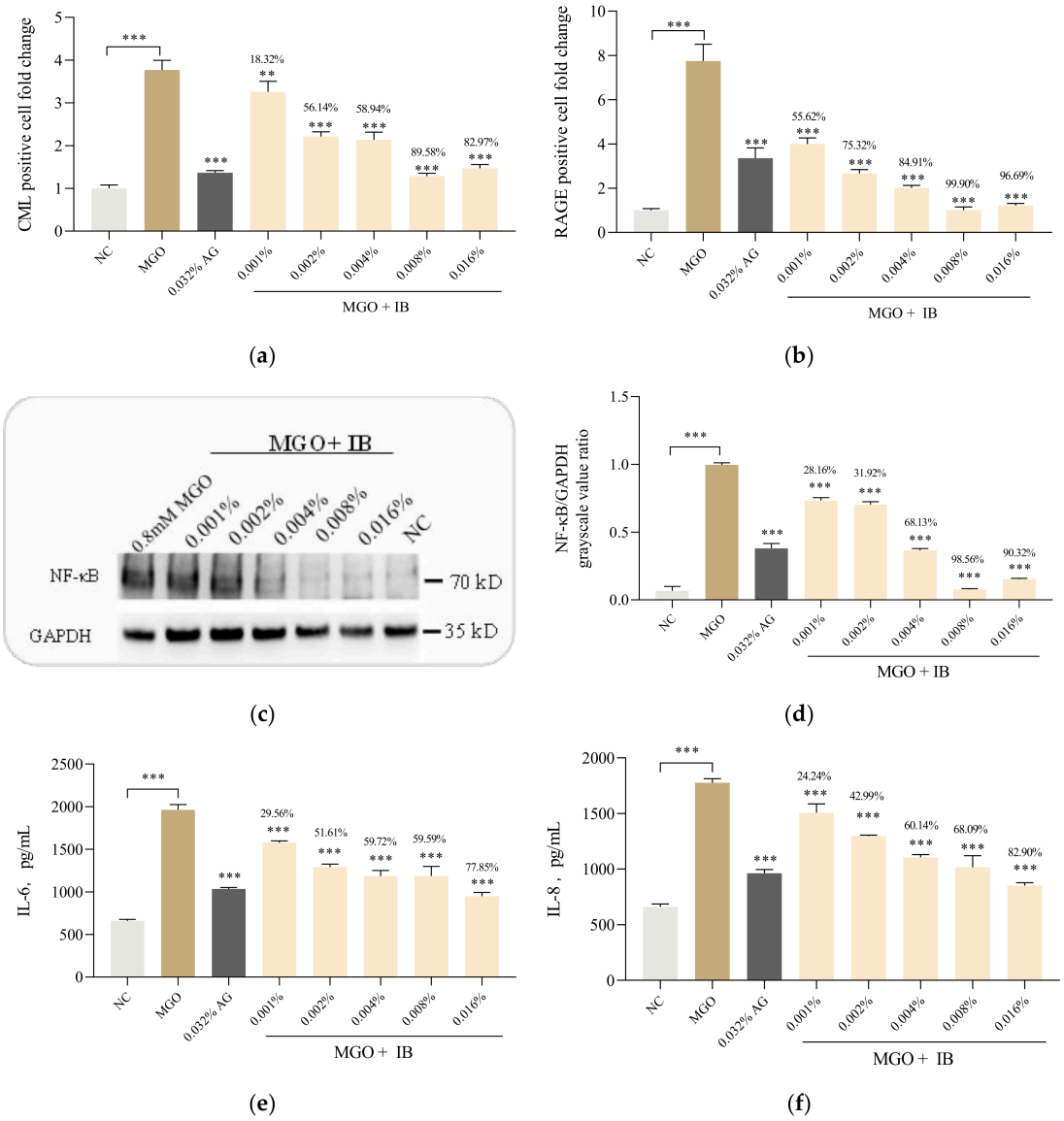


Figure 3. Anti-glycation effects of IB on MGO-induced UVAP7 fibroblasts. UVAP7 dermal fibroblasts were exposed to 0.8 mM MGO for 7 days and co-treated with the indicated concentrations of IB. The proportions of CML-positive (**a**) and RAGE-positive (**b**) cells were determined via flow cytometry. (**c**) Representative immunoblots of NF-κB and GAPDH. (**d**) Densitometric analysis of NF-κB protein expression normalized to GAPDH. IL-6 (**e**) and IL-8 (**f**) contents in culture supernatants were measured via ELISA. Aminoguanidine (AG; 0.032%) was used as the positive control. Data are presented as the mean ± SD ($n = 3$). ** $p < 0.01$; *** $p < 0.001$ vs. MGO group.

3.3. Anti-Ageing Effects of IB Mediated by Inhibiting Glycation

Senescent cells usually have increased cell volume and exhibit high activity of the β-gal enzyme at pH 6.0. SA-β-gal is a biomarker associated with cell senescence, and its expression level is positively correlated with chronic inflammation [16]. In the senescence-associated assays, MGO increased SA-β-gal positivity, accompanied by an induction of the cell cycle inhibitor p16's mRNA expression and a decrease in nuclear lamina LMNB1 mRNA expression (Figure 4). For IB and AG, it significantly inhibited both SA-β-gal positivity and p16 expression, but increased LMNB1 expression, while the vehicle control of hydroxypropyl cyclodextrin had no significant effect. At 0.032%, the inhibition rate was 105.10% for SA-β-gal and 57.01% for p16, and the increase rate reached 92.14% for LMNB1. At 0.016%, the change rate was similar to that at 0.032%, which may have been caused by the complex extract and

the duplicates in the experiment. The SA-β-gal inhibition rate exceeded 100% because of its normalization to NC, which also had some SA-β-gal positive cells.

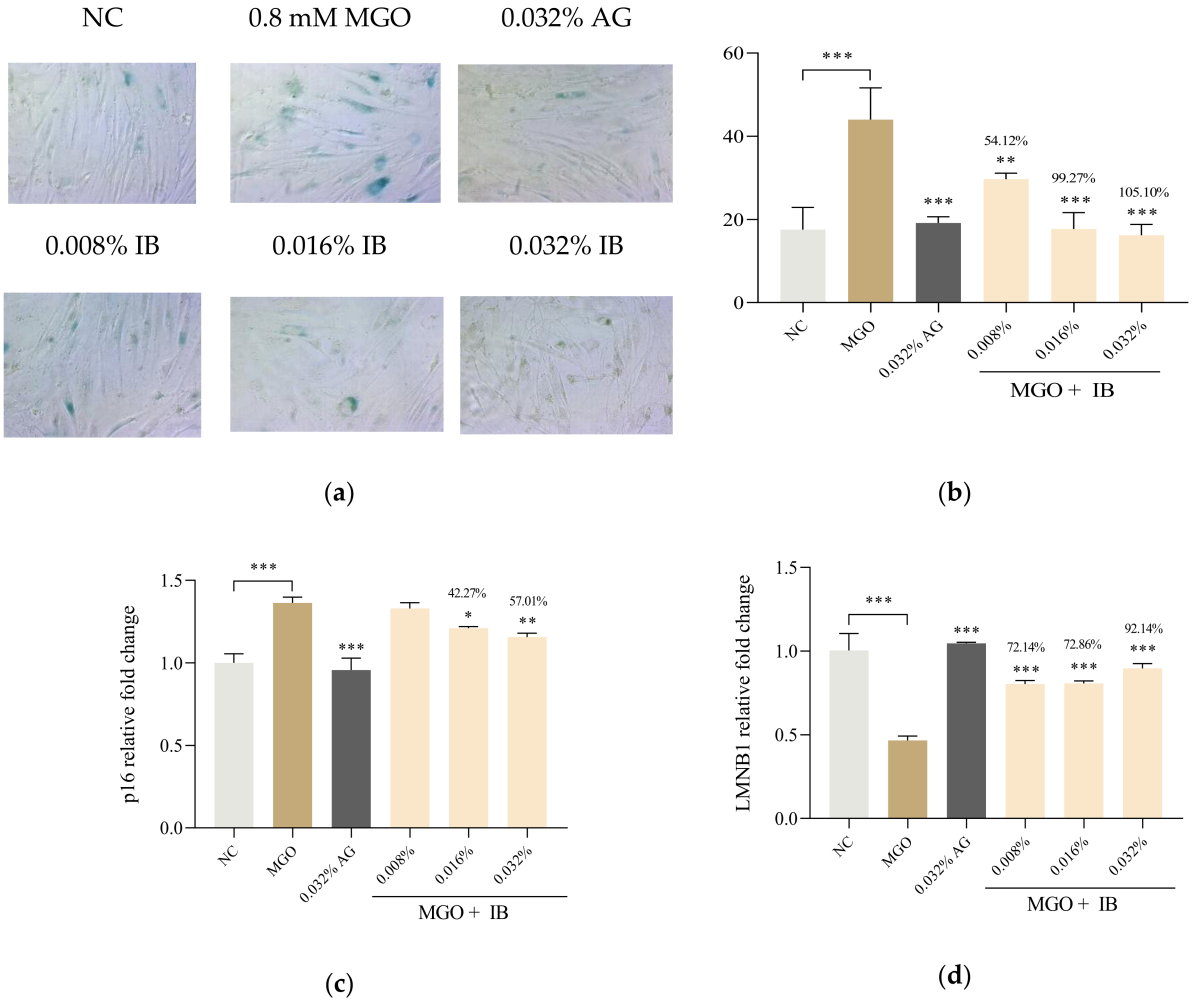


Figure 4. Anti-ageing effects of IB on MGO-induced UVAP7 fibroblasts. UVAP7 dermal fibroblasts were exposed to 0.8 mM MGO for 7 days and co-treated with the indicated concentrations of IB. (**a**) Representative SA-β-gal staining; blue cells are SA-β-gal-positive (original magnification, ×400). (**b**) Percentage of SA-β-gal-positive cells. (**c**,**d**) Relative p16 and LMNB1 mRNA expression, normalized to GAPDH. Aminoguanidine (AG; 0.032%) was the positive control. Data are mean ± SD ($n = 3$). * $p < 0.05$, ** $p < 0.01$, and *** $p < 0.001$ vs. MGO group.

3.4. IB Reduced Age Associations of Skin Autofluorescence AGEs and CIE b Values*

The AGE Reader utilizes an ultraviolet lamp to measure and calculate the ratio between the intensity of emitted light (420–600 nm) and reflected light (300–420 nm) from the skin, to reflect the level of AGEs (glycation) in skin [30]. The CIE b* value quantifies the yellowness of the skin. In the cross-sectional datasets, in all groups aged ≥30 years, the number of skin autofluorescence AGEs was significantly higher than that in the 20–29-year group, whereas the CIE b* values were significantly higher in groups aged ≥40 years (Figure 5a,b). Following linear analysis of the data, age was positively associated with skin autofluorescence AGEs and CIE b* values, providing an equation of linear regression of $y = 0.04327x - 0.1499$ ($R^2 = 0.8003$; $n = 114$) and $y = 0.1166x + 11.78$ ($R^2 = 0.5464$; $n = 162$), shown in Figure 5c and Figure 5d, respectively.

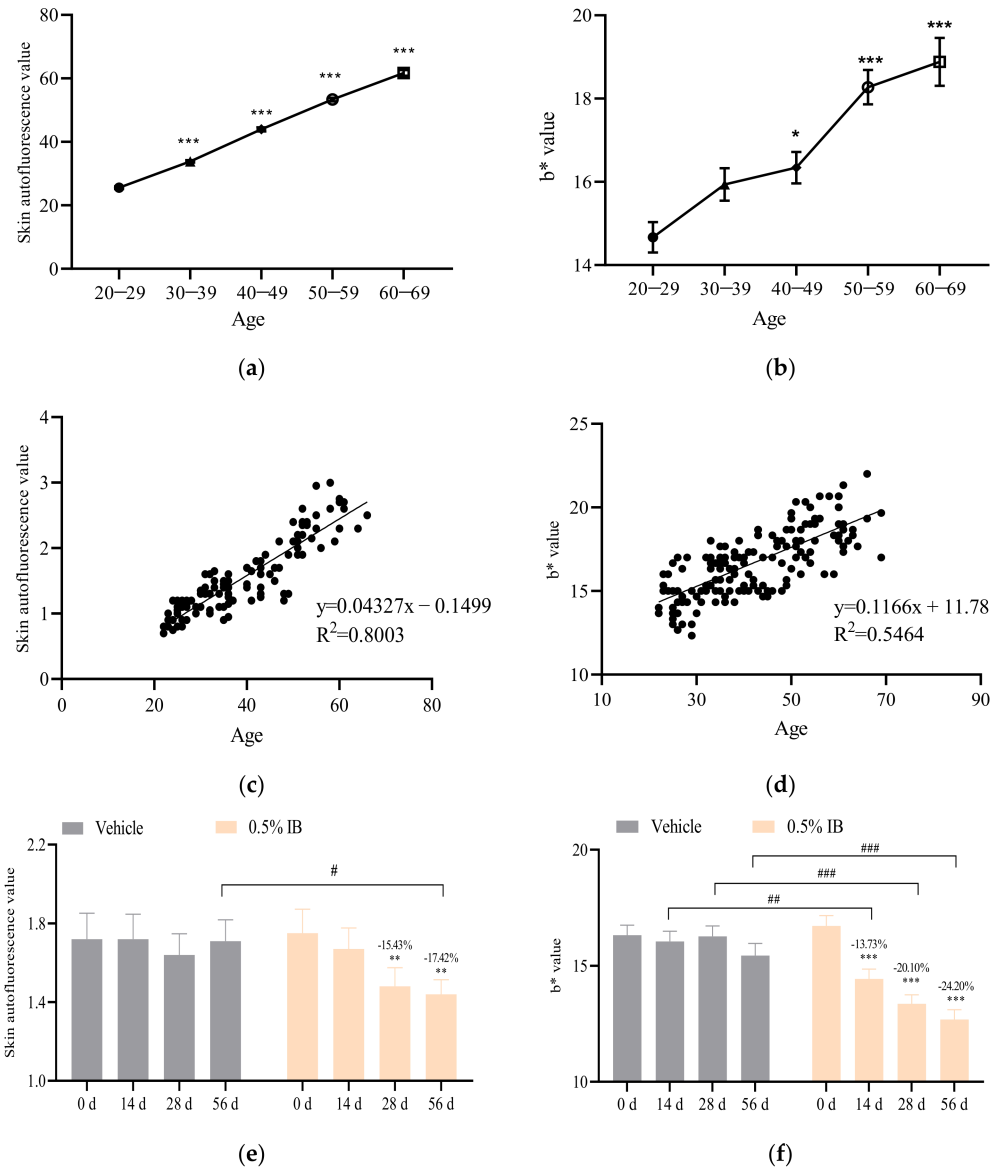


Figure 5. Cross-sectional associations of skin autofluorescence AGEs and CIE b* with age and IB induction. (**a**) Skin autofluorescence AGEs and (**b**) CIE b* value by 10-year age groups. The 20–29-year group was used as the comparison. Linear associations of age with AGEs ((**c**), $n = 114$) and CIE b* value ((**d**), $n = 162$). Lines show fitted regressions; R^2 is the coefficient of determination. (**e**) Skin AGEs and (**f**) CIE b* value at different times after vehicle and IB treatment. Data are shown as mean with SEM. * or $^{\#}$ $p < 0.05$, ** or $^{\#\#}$ $p < 0.01$, and *** or $^{\#\#\#}$ $p < 0.001$.

The test formulas showed no adverse skin reactions in a 24 h pre-study occlusive patch test. As shown in Figure 5e, skin autofluorescence AGEs on the IB-treated side notably decreased by 15.43% on day 28 (28d) and 17.42% on day 56 (56d) from baseline (0d); the value was significantly lower than that on the vehicle-treated side at 56d. As shown in Figure 5f, the CIE b* value notably decreased by 13.73%, 20.10%, and 24.20% at 14d, 28d, and 56d, respectively, compared with 0d, and it was significantly lower than that on the vehicle-treated side at 14d, 28d, and 56d. Post hoc application of the age-equivalent estimates derived from a population regression model to the day 56 changes yielded a predicted age-equivalent differences of approximately 4 years for autofluorescence AGEs and 20 years for the CIE b* value. These changes induced by IB treatment could be clearly observed in the subsequent Vplus imaging and yellowness score reported by the dermatologist changed from 5.39 ± 1.52 (grade 5) at 0d to 4.75 ± 1.68 (grade 4) at 28d ($p < 0.001$).

3.5. IB Ameliorated Signs of Skin Ageing on Wrinkles and Dermal Echogenicity

Skin ageing relates to many characteristics of the face, especially wrinkles and firming [31]. In Figure 6, the scores of under-eye wrinkles significantly decreased by 5.61%, 7.92%, and 9.24%, and the crow's feet scores decreased by 5.35%, 6.29%, and 8.81% after the topical application of 0.5% IB for 14d, 28d, and 56d, respectively. Concurrently, the high-intensity dermal echo increased by 14.88%, 21.12%, and 26.69% on 14d, 28d, and 56d. At 56d, both the under-eye wrinkle scores and crow's feet scores were significantly lower, and the high-intensity echo was significantly higher on the IB-treated side compared with the vehicle-control side. These changes induced by IB treatment could be clearly observed in the subsequent Vplus imaging, and the under-eye wrinkle scores reported by the dermatologist changed from 4.21 ± 1.18 (grade 4) at 0d to 3.88 ± 0.96 (grade 3) at 28d ($p < 0.001$).

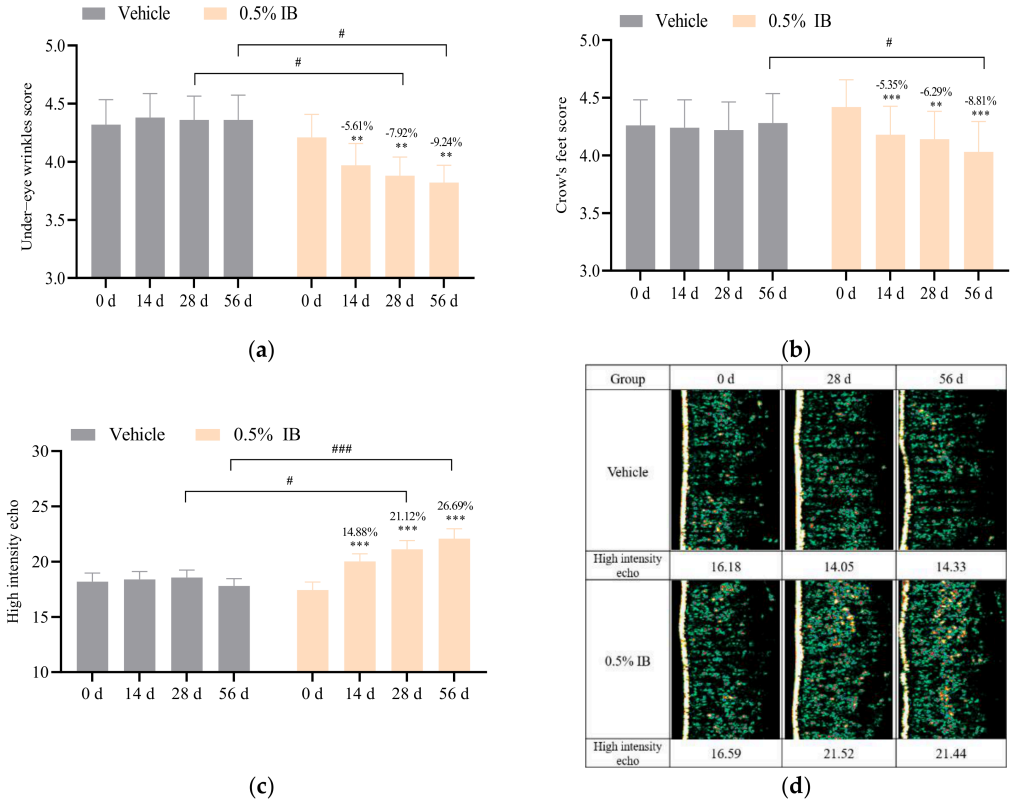


Figure 6. Effects of the 0.5% IB formulation on periocular wrinkles and dermal echogenicity. (**a**) Under-eye wrinkle score, (**b**) crow's feet score, and (**c**) high-intensity dermal echo at different times after vehicle and IB treatment. (**d**) Representative ultrasound images from one participant. Data are shown as mean with SEM. $^{\#}$ $p < 0.05$, ** $p < 0.01$, and *** or $^{\#\#\#}$ $p < 0.001$.

4. Discussion

MGO is a reactive dicarbonyl that promotes the formation of CML and other AGEs. AGEs interacting with RAGE can activate NF-κB-dependent inflammatory signalling, thereby reinforcing the senescence-associated secretory phenotype [3,4,10–15]. But in human dermal fibroblasts, there has been a lack of direct support for MGO-induced glycation and ageing [34]. This study provides a complete chain of evidence demonstrating that MGO induces the formation of AGEs and subsequently activates RAGE, regulating the expression of NF-κB, thus promoting the expression of IL-6 and IL-8 and ultimately accelerating cellular senescence in normal dermal fibroblasts. Among the additional research results that we have not presented, UVAP7 fibroblasts demonstrated greater sensitivity.

When treated with 0.1 to 1 mM MGO for 3 to 7 days, the glycation reaction and cell senescence exhibited dose-dependent and time-dependent patterns. A treatment with 0.8 mM MGO for 7 days was sufficient to cause the irreversible formation of AGEs and to affect downstream signaling. Although the activation of NF-κB needs to be verified with more data, based on previous research [12,35], the activation of RAGE by AGEs could induce the production of reactive oxygen species (ROS), or act through the ERK and Akt pathways to promote or activate the expression of NF-κB, thereby inducing the production of cytokines (Figure 7).

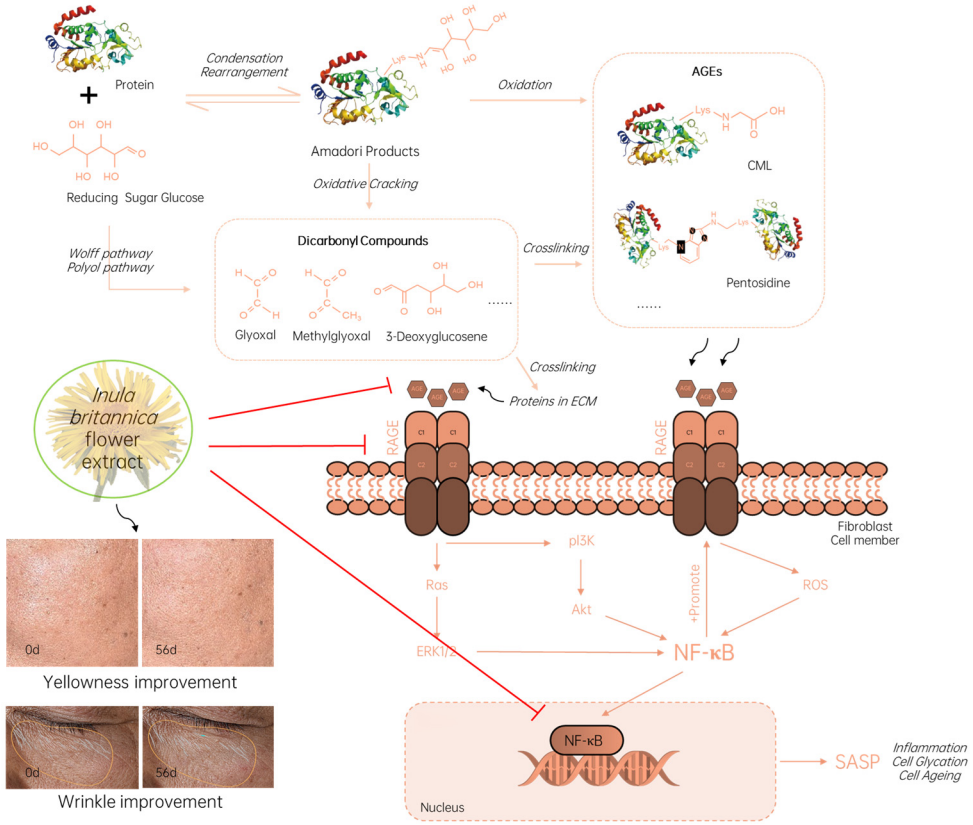


Figure 7. Proposed schema of IB's anti-glycation and well-ageing effects. The distinct colors assign to protein subunits correspond to their respective structural classifications.

Aminoguanidine and carnosine prevented AGE formation by scavenging free radicals in cells [36], but data supporting their downstream targets are lacking. *Inonotus obliquus* polysaccharide showed a protective effect on MGO-induced nonenzymatic glycation human embryonic skin fibroblasts [35], highlighting a potential relationship between AGEs and NF-κB or AP-1. In these MGO-induced UVAP7 fibroblasts, aminoguanidine consistently significantly inhibited the expression of CML, and also inhibited the expression of RAGE, NF-κB, IL-6, IL-8, and p16, supressing glycation and cell senescence. Therefore, despite certain limitations, the results observed for UVAP7 cells could reflect the effects and mechanisms of anti-glycation compounds.

Considering *Inula britannica* flower extract, its total flavonoids were reported to inhibit RAGE expression under L929 cell ageing induced by AGEs [37] and inhibit D-galactose-induced ageing in mice [28]. There is little data on its anti-glycation and anti-ageing effects in MGO-challenged human dermal fibroblasts. In this study, IB was found to contain many phenols but few flavonoids. For instance, the contents of nepetin, luteolin, and quercetin (peaks 39, 38, and 18 in Figure 2a) were all lower than 0.001%, while the contents of 1,3-dicaffeoylquinic acid, 1,5-dicaffeoylquinic acid, isochlorogenic acid A, and isochlorogenic

acid C were all higher than 0.1%. IB was firstly found to inhibit skin glycation by reducing the expression of RAGE and NF-κB, as well as the expression of IL-6 and IL-8. Furthermore, IB downregulated SA-β-gal-positive cells, suppressed p16 gene expression, and increased LMNB1 gene expression, which are typical features in cellular senescence [16,17]. The coordinated response across these endpoints indicated that IB attenuated MGO-induced cell glycation and ageing, though this is not attributed solely to flavonoids. The caffeoylquinic and caffeoylglucaric acid derivatives detected in the extract may provide a plausible phytochemical basis because phenolics have demonstrated anti-glycation [19–22], antioxidant, and anti-inflammatory activities [38–40]. Additionally, 1,3-dicaffeoylquinic acid showed a good free radical scavenging effect and inhibited the MGO-inducted glycation of collagen. Some cellular endpoints did not show a strictly monotonic concentration–response relationship, with the largest effect occurring below the highest tested concentration. This pattern may reflect response saturation, interactions among extract constituents, or assay variability and should be examined in expanded dose–response experiments or with an increased number of test replicates.

Skin autofluorescence AGEs are an optical marker associated with cutaneous AGEs accumulation. The parallel reduction in CIE b* value was consistent with an improvement in the yellow colour component linked to the accumulation of glycation-derived chromophores in ageing skin [5–8]. Cross-sectional associations of both endpoints with age further supported their relevance to skin ageing. The darker the skin, the higher the autofluorescence AGEs and CIE b* value, and the higher the content of CML in the skin [41,42]. At present, there is no evidence to prove the efficacy of IB in human skin. In this split-face study, the formulation containing 0.5% IB significantly decreased the skin autofluorescence AGEs, CIE b* values, periocular wrinkle scores, but significantly increased the dermal echogenicity after topical application for 56 days when compared to the vehicle, indicating improvements for facial yellowness and ageing. The 56-day between-side differences in periocular wrinkle scores and yellowness scores extend the clinical effect to structural and visible features. The cellular and clinical findings form a coherent translational evidence chain. Reduced CML and RAGE responses in fibroblasts contribute to lower cytokines and improvements in cell ageing, accompanied clinically by lower yellowness and wrinkles. Although the results obtained in vitro provide more explanations of the mechanism, and the test concentrations need to be supported by results for transdermal absorption to reflect application in vivo, these findings support a multi-target effect extending from glycation-related cellular responses to measurable changes in human skin.

On the age-equivalent estimates derived from a population regression model, using IB for 56 days yielded age-equivalent differences of approximately 4 years for autofluorescence AGEs and 20 years for the CIE b* value. The association with age was weaker for CIE b* than for autofluorescence, because facial colour is influenced by melanin, hemoglobin, vascularity, and environmental exposure in addition to glycation. Accordingly, the age-equivalent estimates are best used to contextualize the effect size rather than to imply the reversal of biological age. Similarly, this study also has certain limitations. The clinical study was single-centre, used a fixed side allocation, and had a 56-day follow-up period. Only the subjects and dermatologist were blinded, while the clinical assessor was not, and a prespecified multiplicity control is not reported. Further chemical standardization and confirmatory clinical studies are needed to confirm the application of IB.

5. Conclusions

Inula britannica flower extract attenuates MGO-induced glycation and senescence-related responses in dermal fibroblasts by inhibiting AGE formulation, RAGE expression, NFκB expression, and cytokine contents, improving skin yellowness, periocular wrinkles,

and echogenicity relative to the vehicle. These findings support the further investigation of this chemically standardized extract and its potential application in skin ageing. Other mechanisms of this extract will be further investigated. Multi-centre tests with randomized, double-blinded, and large-scale populations should also be conducted.

Author Contributions: Conceptualization, Y.L. and X.L.; Methodology, F.Z. and X.L.; Software, F.Z.; Validation, F.Z., X.L. and L.X.; Formal Analysis, F.Z.; Investigation, Z.Y.; Resources, Y.L. and F.-Q.W.; Data Curation, F.Z.; Writing—Original Draft Preparation, Y.L.; Writing—Review & Editing, Z.Y. and F.-Q.W.; Visualization, Y.L.; Supervision, F.-Q.W.; Project Administration, Y.L.; Funding Acquisition, Y.L. and F.-Q.W. All authors have read and agreed to the published version of the manuscript.

Funding: This research received no external funding.

Institutional Review Board Statement: The study was conducted in accordance with the Declaration of Helsinki, and approved by the Ethics Committee of Cosmetics Evaluation Ethics Committee of JAKA (protocol code JKC-2412-00055 and date of approval at 24 December 2024).

Informed Consent Statement: Informed consent was obtained from all subjects involved in the study.

Data Availability Statement: The data presented in this study are available on request from the corresponding author due to privacy and ethical reasons. The original contributions presented in this study are included in the article.

Acknowledgments: The authors thank all individuals who participated in this study.

Conflicts of Interest: Y.L., F.Z., X.L. and L.X. are employed by JAKA Biotech Co., Ltd. The company participated in the design of the study; in the collection, analyses or interpretation of data; in the writing of the manuscript; or in the decision to publish the results.

References

1. Thau, H.; Gerjol, B.P.; Hahn, K.; von Gudenberg, R.W.; Knoedler, L.; Stallcup, K.; Emmert, M.Y.; Buhl, T.; Wyles, S.P.; Tchkonia, T.; et al. Senescence as a molecular target in skin aging and disease. *Ageing Res. Rev.* **2025**, *105*, 102686. [CrossRef]
2. Costello, L.; Dicolandrea, T.; Tassef, R.; Isfort, R.; Bascom, C.; von Zglinicki, T.; Przyborski, S. Tissue engineering strategies to bioengineer the ageing skin phenotype in vitro. *Aging Cell* **2022**, *21*, e13550. [CrossRef]
3. Zhu, J.; Wang, Z.; Lv, C.; Li, M.; Wang, K.; Chen, Z. Advanced glycation end products and health: A systematic review. *Ann. BioMed. Eng.* **2024**, *52*, 3145–3156. [CrossRef]
4. Sroga, G.E.; Vashishth, D. In vivo glycation-interplay between oxidant and carbonyl stress in bone. *JBMR Plus* **2024**, *8*, ziae110. [CrossRef]
5. Choi, J.Y.; Ha, N.G.; Lee, W.J.; Boo, Y.C. Synthetic and natural agents targeting advanced glycation end-products for skin anti-aging: A comprehensive review of experimental and clinical studies. *Antioxidants* **2025**, *14*, 498. [CrossRef]
6. Zheng, W.; Li, H.; Go, Y.; Chan, X.H.F.; Huang, Q.; Wu, J. Research advances on the damage mechanism of skin glycation and related inhibitors. *Nutrients* **2022**, *14*, 4588. [CrossRef]
7. Crisan, M.; Taulescu, M.; Crisan, D.; Cosgarea, R.; Parvu, A.; Catoi, C. Expression of advanced glycation end-products on sun-exposed and non-exposed cutaneous sites during the ageing process in humans. *PLoS ONE* **2013**, *8*, e75003. [CrossRef]
8. Knoblich, C.; Dunckelmann, K.; Krüger, A.; Küper, T.; Blatt, T.; Weise, J.M. N-acetyl-L-hydroxyproline-A potent skin anti-ageing active preventing advanced glycation end-product formation in vitro and ex vivo. *Int. J. Cosmet. Sci.* **2024**, *46*, 297–306. [CrossRef]
9. Mengstie, M.A.; Chekol, A.E.; Behaile, T.A.; Tilahun, M.A.; Agidew, M.M.; Teshome, A.M.; Zewde, E.A.; Agegnehu, T.A. Endogenous advanced glycation end products in the pathogenesis of chronic diabetic complications. *Front Mol. Biosci.* **2022**, *9*, 1002710. [CrossRef]
10. Cross, K.; Vetter, S.W.; Alam, Y.; Hasan, M.Z.; Nath, A.D.; Leclerc, E. Role of the receptor for advanced glycation end products (RAGE) and its ligands in inflammatory responses. *Biomolecules* **2024**, *14*, 1550. [CrossRef]
11. Ramasamy, R.; Yan, S.F.; Schmidt, A.M. RAGE: Therapeutic target and biomarker of the inflammatory response—The evidence mounts. *J. Leukoc. Biol.* **2009**, *86*, 505–512. [CrossRef]
12. Chen, C.Y.; Zhang, J.Q.; Li, L.; Guo, M.M.; He, Y.F.; Dong, Y.M.; Meng, H.; Yi, F. Advanced glycation end products in the skin: Molecular mechanisms, methods of measurement, and inhibitory pathways. *Front. Med.* **2022**, *9*, 837222. [CrossRef]
13. Deepu, V.; Rai, V.; Agrawal, D.K. Quantitative assessment of intracellular effectors and cellular response in RAGE activation. *Arch. Intern Med. Res.* **2024**, *7*, 80–103. [CrossRef]

14. Takasugi, M.; Yoshida, Y.; Ohtani, N. Cellular senescence and the tumour microenvironment. *Mol. Oncol.* **2022**, *16*, 3333–3351. [CrossRef]
15. Ikegami, K.; Yamashita, M.; Suzuki, M.; Nakamura, T.; Hashimoto, K.; Kitagaki, J.; Yanagita, M.; Kitamura, M.; Murakami, S. Cellular senescence with SASP in periodontal ligament cells triggers inflammation in aging periodontal tissue. *Aging* **2023**, *15*, 1279–1305. [CrossRef]
16. Dorf, N.; Maciejczyk, M. Skin senescence-from basic research to clinical practice. *Front. Med.* **2024**, *11*, 1484345. [CrossRef]
17. Freund, A.; Laberge, R.M.; Demaria, M.; Campisi, J. Lamin B1 loss is a senescence-associated biomarker. *Mol. Biol. Cell* **2012**, *23*, 2066–2075. [CrossRef]
18. Reddy, V.P.; Aryal, P.; Darkwah, E.K. Advanced glycation end products in health and disease. *Microorganisms* **2022**, *10*, 1848. [CrossRef]
19. Fernandes, A.C.F.; Melo, J.B.; Genova, V.M.; Santana, Á.L.; Macedo, G. Phytochemicals as potential inhibitors of advanced glycation end products: Health aspects and patent survey. *Recent Adv. Food Nutr. Agric.* **2022**, *13*, 3–16. [CrossRef]
20. Sadowska-Bartosz, I.; Bartosz, G. Prevention of protein glycation by natural compounds. *Molecules* **2015**, *20*, 3309–3334. [CrossRef]
21. Zhao, L.; Zhu, X.; Yu, Y.; He, L.; Li, Y.; Zhang, L.; Liu, R. Comprehensive analysis of the anti-glycation effect of peanut skin extract. *Food Chem.* **2021**, *362*, 130169. [CrossRef]
22. Yeh, W.J.; Hsia, S.M.; Lee, W.H.; Wu, C.H. Polyphenols with antiglycation activity and mechanisms of action: A review of recent findings. *J. Food Drug Anal.* **2017**, *25*, 84–92. [CrossRef]
23. Yang, L.; Wang, X.; Hou, A.; Zhang, J.; Wang, S.; Man, W.; Yu, H.; Zheng, S.; Wang, Q.; Jiang, H.; et al. A review of the botany, traditional uses, phytochemistry, and pharmacology of the Flos Inulae. *J. Ethnopharmacol.* **2021**, *276*, 114125. [CrossRef]
24. Khan, A.L.; Hussain, J.; Hamayun, M.; Gilani, S.A.; Ahmad, S.; Rehman, G. Secondary metabolites from *Inula britannica* L. and their biological activities. *Molecules* **2010**, *15*, 1562–1577. [CrossRef]
25. Ibadullayeva, A.K.; Kasela, M.; Kozhanova, K.K.; Kadyrbayeva, G.M.; Widelski, J.; Wojtanowski, K. Chemical profile and biological properties of methanolic and ethanolic extracts from the aerial parts of *Inula britannica* L. growing in Central Asia. *Molecules* **2024**, *29*, 5749. [CrossRef]
26. Ivanova, V.; Trendafilova, A.; Todorova, M.; Danova, K.; Dimitrov, D. Phytochemical profile of *Inula britannica* from Bulgaria. *Nat. Prod. Commun.* **2017**, *12*, 153–154. [CrossRef]
27. Jeon, J.M.; Yoo, D.S.; Cheon, J.W.; Kwon, S.S.; Jeon, S.H.; Park, S.N. Anti-aging effect of *Inula britannica* var. *chinensis* flower extract according to the extraction temperature. *J. Soc. Cosmet. Sci. Korea* **2014**, *40*, 109–120. [CrossRef]
28. Chen, H.; Long, Y.; Guo, L. Antiaging effect of *Inula britannica* on aging mouse model induced by D-galactose. *Evid. Based Complement Altern. Med.* **2016**, *2016*, 6049083. [CrossRef]
29. Henrot, P.; Laurent, P.; Levionnois, E.; Leleu, D.; Pain, C.; Truchetet, M.E. A method for isolating and culturing skin cells: Application to endothelial cells, fibroblasts, keratinocytes, and melanocytes from punch biopsies in systemic sclerosis skin. *Front. Immunol.* **2020**, *11*, 566607. [CrossRef]
30. *T/ZHCA 026-2023*; Clinical Method for Evaluation of Antiglycation Cosmetic Products. ZheJiang Health Products & Cosmetics Industry Association: Hangzhou, China, 2023.
31. *TB/ZGKSL 001-2022*; Evaluation Criteria for Human Skin Aging. China Anti-Aging Promoting Association: Beijing, China, 2022.
32. Zhou, L.D.; Lu, Y.N.; Gao, Y.; Xiong, Y.; Shi, X.M. Method for Constructing Senescent Cells and Method for Evaluating Anti-Senescence Efficacy. U.S. Patent 18,857,906, 2026.
33. Markiewicz, E.; Jerome, J.; Mammone, T.; Idowu, O.C. Anti-glycation and anti-aging properties of resveratrol derivatives in the in-vitro 3D models of human skin. *Clin. Cosmet. Investig. Dermatol.* **2022**, *15*, 911–927. [CrossRef]
34. Serban, A.I.; Stanca, L.; Geicu, O.I.; Munteanu, M.C.; Dinischiotu, A. RAGE and TGF-β1 cross-talk regulate extracellular matrix turnover and cytokine synthesis in ages exposed fibroblast cells. *PLoS ONE* **2016**, *11*, e0152376. [CrossRef]
35. Chen, C.; Liu, X.; Lin, Y.; Li, L.; Guo, M.; Yi, F. Protective effect of *Inonotus obliquus* polysaccharide on MGO-induced nonenzymatic glycation fibroblasts. *Heliyon* **2024**, *10*, e27458. [CrossRef]
36. Khan, M.R.; Khan, M.S.; Manoharan, R.; Karthikeyan, S.; Alhosaini, K.; Odeibat, H.A.M.; Ahmad, M.D.I.; Al-Okail, M.; Al-Twaijry, N. Inhibitory potential of carnosine and aminoguanidine towards glycation and fibrillation of albumin: In-vitro and simulation studies. *J. Fluoresc.* **2025**, *35*, 29–42.
37. Liu, L.; Long, Y.Y.; Guo, Z.Y.; Tang, W.; Guo, L. *Inula britannica* flower total flavonoids inhibiting expression of RAGE in aging L929 cells induced by advanced glycation end products. *Chin. Tradit. Herb. Drugs* **2018**, *49*, 626–632.
38. Alcázar Magaña, A.; Kamimura, N.; Soumyanath, A.; Stevens, J.F.; Maier, C.S. Caffeoylquinic acids: Chemistry, biosynthesis, occurrence, analytical challenges, and bioactivity. *Plant J.* **2021**, *107*, 1299–1319. [CrossRef]
39. Jang, G.; Lee, S.; Hong, J.; Park, B.; Kim, D.; Kim, C. Anti-inflammatory effect of 4,5-dicaffeoylquinic acid on RAW264.7 cells and a rat model of inflammation. *Nutrients* **2021**, *13*, 3537. [CrossRef]

40. Dudek, M.K.; Dudkowski, Ł.; Bazylko, A.; Kaźmierski, S.; Kiss, A.K. Caffeic acid derivatives isolated from the aerial parts of *Galinsoga parviflora* and their effect on inhibiting oxidative burst in human neutrophils. *Phytochem. Lett.* **2016**, *16*, 303–310. [CrossRef]
41. Laughlin, T.; Tan, Y.; Jarrold, B.; Chen, J.; Li, L.; Fang, B.; Zhao, W.; Tamura, M.; Matsubara, A.; Deng, G.; et al. Autophagy activators stimulate the removal of advanced glycation end products in human keratinocytes. *J. Eur. Acad. Dermatol. Venereol.* **2022**, *34*, 12–18.
42. Fournet, M.; Bonté, F.; Desmoulière, A. Glycation damage: A possible hub for major pathophysiological disorders and aging. *Aging Dis.* **2018**, *9*, 880–900. [CrossRef]

Disclaimer/Publisher's Note: The statements, opinions and data contained in all publications are solely those of the individual author(s) and contributor(s) and not of MDPI and/or the editor(s). MDPI and/or the editor(s) disclaim responsibility for any injury to people or property resulting from any ideas, methods, instructions or products referred to in the content.